HKUST

DATASET · AUGUST 2014

READS
35

7 AUTHORS, INCLUDING:

Hao Chen
Texas A&M University
18 PUBLICATIONS **125** CITATIONS
SEE PROFILE

Min-Hao Yuan
University of Michigan
15 PUBLICATIONS **104** CITATIONS
SEE PROFILE

Sandrine Rivillon
Air Products and Chemicals
40 PUBLICATIONS **852** CITATIONS
SEE PROFILE

THE JOURNAL OF PHYSICAL CHEMISTRY C

Article

pubs.acs.org/JPCC

Investigation on Hydrogenation of Metal−Organic Frameworks HKUST-1, MIL-53, and ZIF-8 by Hydrogen Spillover

Hao Chen,[†] Lifeng Wang,[†] Jun Yang,[‡] and Ralph T. Yang*[,†]

[†]Department of Chemical Engineering, University of Michigan, Ann Arbor, Michigan 48109, United States

[‡]Research and Advanced Engineering, Ford Motor Company, MD1170/RIC, Dearborn, Michigan 48121, United States

Supporting Information

ABSTRACT: The stabilities of three moisture-stable MOFs containing different metal clusters, i.e., HKUST-1 (Cu), MIL-53(Al), and ZIF-8 (Zn), were investigated in dihydrogen and dissociated hydrogen (caused by doped Pt nanoparticles) environments. X-ray diffraction (XRD), X-ray photoelectron spectroscopy (XPS), and X-ray-excited Auger electron spectroscopy (XAES) results showed that all three MOFs were stable in dihydrogen environment. However, the structure of Pt-doped HKUST-1 collapsed in the presence of dissociated hydrogen due to the higher reduction potential of Cu compared with H, and the degree of reduction that occurred to the divalent copper in HKUST-1 increased with temperature. Unlike HKUST-1, MIL-53 and ZIF-8 maintained their structures in both dihydrogen and dissociated hydrogen environments at temperatures up to 150 °C. Moreover, comparison of Pt-doped HKUST-1 samples synthesized by chemical vapor deposition (CVD) and incipient wetness impregnation showed that the contact between the doped Pt particles (dissociation source) and MOFs (receptor) significantly affected hydrogen spillover.

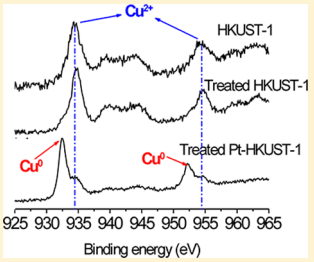

1. INTRODUCTION

Hydrogen is considered as one promising alternative energy carrier for environmental sustainability.[1] Among many factors hindering the wide deployment of hydrogen as hydrocarbon fuel substitution, hydrogen storage is one of the key issues for commercialization of fuel cell powered vehicles using hydrogen as energy carrier due to the low volumetric energy density of hydrogen, which is only 1/3000 of the volumetric energy density of gasoline.[2] Many adsorbent materials have been developed as possible candidates for hydrogen storage over the past few decades.[3−10] Among these candidates, metal−organic frameworks (MOFs), a class of porous crystalline materials consisting of metal ions or metal containing clusters coordinated to rigid organic molecules to form one-, two-, or three-dimensional structures, have attracted much attention because of their light weight, exceptional high surface area, high porosity, and chemically tunable structures.[11−28]

There has been an intense search for MOFs with high hydrogen storage capacities. Significant progress has been achieved for hydrogen storages at 77 K. For example, MIL-101 with a Langmuir surface area of 5500 m^2/g possessed a storage capacity of 6.1 wt % at 8 MPa and 77 K.[29] The hydrogen adsorption capacity at 77 K by MOF-177 (BET surface area 4750 m^2/g) and UMCM-2 (BET surface area 5200 m^2/g) reached 7.5 wt % at 7 MPa and 7 wt % at 6 MPa, respectively.[30,31] Furukawa et al. reported MOF-210 with a record BET surface area of 6240 m^2/g and a hydrogen capacity of 8.6 wt % at 77 K and 8 MPa.[32] More recently, Farha et al. reported that NU-100, which has a slightly smaller surface area (BET 6143 m^2/g) but much higher hydrogen storage capacity (9.95 wt % at 77 K and 6 MPa).[33] The MOF with highest surface area so far was NU-110, with a BET SA 7140 m^2/g, but no hydrogen uptake capacity reported.[34] However, these significant storage capacities were achieved only at 77 K, and they declined dramatically when the temperature was raised to ambient temperature. This is understandable since hydrogen adsorption on pristine MOFs was by weak physisorption and mainly dominated by weak van der Waals interactions.

In order to improve the performance of adsorbent materials for hydrogen storage at ambient temperature, an effective approach was proposed by utilizing hydrogen dissociation on metal surface followed by spillover. General concept of hydrogen spillover could be defined as dissociative chemisorptions of hydrogen on metal nanoparticles and subsequent migration of dissociated hydrogen atoms onto adjacent receptor surfaces via diffusion.[35−38] Up to date, over 140 papers published by more than 50 groups have demonstrated the effectiveness of utilizing hydrogen spillover for storage enhancement on adsorbents at room temperature.[39] First evidence of atomic hydrogen spillover was observed by Sinfelt and Lucchesi in studies of ethylene hydrogenation by H atoms spillover from Pt/SiO_2 to Al_2O_3.[40] Later, Khoobiar showed WO_3 in contact with a Pt catalyst could be reduced by H_2 to blue WO_{3-x}.[41] In 1971, Pajonk and Teichner found that a pure support (Al_2O_3 or SiO_2) treated with H_2 for several hours at elevated temperature can hydrogenate ethylene and benzene even by indirect contact with a supported metal catalyst.[42] Reduction of transition metal oxide with Pt catalyst has been used as the proof of hydrogen spillover by Khoobiar, Bourdart, and Bond et al.[41,43−45] Direct experimental evidence of atomic

Received: November 30, 2012
Revised: March 23, 2013
Published: March 27, 2013

   dx.doi.org/10.1021/jp401367k | J. Phys. Chem. C 2013, 117, 7565−7576

hydrogen spillover at room temperature have been recently reported in many systems (Pt−carbon,[46−50] Pt-glass,[51] and Au−TiO_2[52,53]) by using inelastic neutron scattering, XPS, nanoelectrochemcial approaches, and FT-IR. Meanwhile, atomistic simulations have also demonstrated the feasibility of hydrogen spillover from metal clusters to receptors. Cheng et al. found migration of H atoms from a Pt cluster catalyst to graphitic carbon substrates occurs via physisorbed of H atoms at room temperature by using DFT calculations.[54,55] The works from Yakobson's group illustrated thermodynamic and kinetic possibility of hydrogen spillover process at room temperature from unsupported or the receptor-supported clusters to graphene sheet through *ab initio* calculations.[56,57] Zhang and co-workers demonstrated the presence of zinc vacancies in IRMOFs could substantially lower the energies and barriers to enable hydrogen spillover at ambient conditions,[58] which is consistent with experiment results that defects in MOFs play an important role in hydrogen spillover at ambient temperature.[59] Moreover, hydrogen storage capacities via spillover for various MOFs and COFs have been calculated.[58,60−65]

Three major approaches have been reported to facilitate hydrogen spillover on MOFs, which is building carbon bridges between dissociation metals and MOFs,[59,60,66−70] encapsulating Pt/C sources into frameworks of MOFs during synthesis,[71,72] and direct doping dissociation metals (Pt, Pd, Ni) onto MOFs.[73−78] Many factors could affect the reproducibility of hydrogen spillover enhancement by bridge-building, and it was suggested the ideal situation for hydrogen spillover on bridged MOFs was all individual catalyst connected with MOF particles via "bridges", which was highly empirical and difficult to achieve.[68] Unlike high uncertainty of the MOF-bridging technique, direct doping metals onto MOFs attracted much attention because of more controllable and reliable synthesis procedure, which led to higher reproducibility. Significant storage capacity enhancements via direct metal doping have been reported by many groups. Suh and co-workers have developed novel methods for producing metal nanoparticles in MOFs by using redox reactions between the redox-active MOFs and metal ions such as Ag(I), Au(III), and Pd(II).[76,79,80] They demonstrated palladium nanoparticles could be embedded into a redox-active MOF simply by immersion of the MOF solid into $Pd(NO_3)_2$ solution at room temperature without further reduction and observed an enhancement factor of 2.3 at 298 K and 9.5 MPa.[76] Our group synthesized a series of Pt-doped IRMOF-8 via organometallic chemical-vapor deposition and observed enhancements from 10 to 100% depending on the particle size.[78] Hydrogen uptake enhancements were also observed on Ni-doped MIL-101,[73] Pt-doped MOF-177,[74] Pd-doped MIL-100,[75] Pd-doped MOF-5,[77] and Pd-doped COF-102.[81]

The recent review from Suh's group summarized different designs and synthesis approaches of MOFs for hydrogen storage, discussed the strategies for improving hydrogen adsorption on MOFs, and reviewed various techniques and methods for hydrogen sorption experiments.[82] They also pointed out that the discovery of a MOF with a large surface and high H_2 adsorption energy at room temperature does not guarantee it will be useful as a H_2 storage material, since industrial applications of MOFs require MOFs to remain stable against moisture, air, and other gas impurities.[82] Thermal stabilities in inert gas and moisture/air/chemical resistance of MOFs have been studied by many researchers.[83−91] Walton and co-workers presented experimental investigations of water adsorption in MOFs at room temperature and up to 90% relative humidity, which demonstrated HKUST-1, MOF-74, and UiO-66 maintained good structural stability against moisture while DMOF-1, DMOF-1-NH_2, and UMCM-1 underwent complete loss of crystallinity.[90] Meanwhile, they also suggested that the thermal stability of MOFs is determined by the coordination number and local coordination environment instead of framework topology by applying TGA-DSC measurements in helium.[91] However, the stabilities of MOFs in hydrogen atmosphere were seldom investigated. Lueking's group mixed HKUST-1 with commercial Pt/C catalyst and observed that hydrogenation of HKUST-1 happened to the carboxylate groups and not aromatic carbons, but the state of metal clusters after hydrogenation still remains unknown.[92] Since MOFs are promising candidate materials for hydrogen storage, it is important to understand MOFs' stabilities in hydrogen atmosphere. Dissociated hydrogen possesses stronger chemical reactivity than dihydrogen molecules; thus, stability of MOFs in the presence of dissociated hydrogen remains an issue especially when spillover of hydrogen is applied to enhance hydrogen storage capacity of pristine MOFs. In this work, the stabilities of three types of moisture stable MOFs with different metal clusters, i.e., HKUST-1 (Cu), MIL-53 (Al), and ZIF-8 (Zn), were studied in dihydrogen and dissociated hydrogen environments. To induce dissociated hydrogen to these MOFs, colloidal Pt nanoparticles were doped on MOFs via incipient wetness for the first time. The influence of dissociated hydrogen and dihydrogen molecules on the stabilities of MOFs with different metal clusters was investigated and compared. The stabilities of Pt-doped HKUST-1 samples synthesized by chemical vapor deposition (CVD) and incipient wetness were also compared to see the effect of contact between doped Pt particles (dissociation source) and MOFs (receptor) on hydrogen spillover.

2. EXPERIMENTAL METHODS

2.1. Sample Synthesis. Copper(II) nitrate hemipentahydrate, $Cu(NO_3)_2{\cdot}2.5H_2O$, NaOH, benzene-1,3,5-tricarboxylic acid (H_3-BTC), hexachloroplatinic acid, $H_2PtCl_6{\cdot}6H_2O$ (99.9%, metals basis), MIL-53(Al) (Basolite A100), ZIF-8 (Basolite Z1200), ethanol, *N*,*N*-dimethylformamide (DMF), ethylene glycol, and chloroform were obtained from Sigma-Aldrich. Helium, nitrogen, and ultrahigh purity grade hydrogen (99.995%) were obtained from Metro Welding Co.

2.1.1. Synthesis of HKUST-1. Typically, 1 g of $Cu(NO_3)_2{\cdot}2.5H_2O$ and 0.5 g of H_3-BTC were dissolved in 25 mL of solvent consisting of equal parts of deionized water, ethanol, and DMF. The mixture was stirred for 15 min at room temperature and then transferred into a Pyrex bottle. The bottle was tightly capped and placed in an 85 °C oven for 20 h to yield small octahedral crystals. After decanting the mother liquor and rinsing with DMF, the product was immersed in chloroform for 1 day, after which the activation solvent was decanted and new chloroform was replenished. This solvent exchange procedure was repeated for three times, and HKUST-1 was filtered and calcined under vacuo at 160 °C to remove excessive solvent, yielding the porous material.[18,93,94]

2.1.2. Synthesis of Platinum Nanoparticles. A routine method for Pt nanoparticle synthesis by using polyol reduction has been reported in previous literature.[95−97] A brief introduction is given here. Typically, 0.25 g of NaOH and 0.25 g of $H_2PtCl_6{\cdot}6H_2O$ was separately dissolved and stirred in two parts of 12.5 mL of ethylene glycol at room temperature.

dx.doi.org/10.1021/jp401367k | J. Phys. Chem. C 2013, 117, 7565−7576

After that, the solution of platinum precursor was slowly dropped into NaOH solution. The solution mixture was kept well-stirred for 30 min at room temperature and then heated at 160 °C for 3 h being accompanied by N_2 bubbling. During this process, the solution turned from yellow color into dark brown. A 6 mL aliquot of the resulting solution was transferred to a vial. The particles were precipitated by adding 1 mL of 2 M HCl into the solution, followed by being washed in ethanol and finally obtained by a high-speed centrifuge.

2.1.3. Synthesis of Pt-HKUST-1, Pt-MIL-53, and Pt-ZIF-8 via Incipient Wetness. HKUST-1 was dried in vacuo at 160 °C overnight before usage while MIL-53 and ZIF-8 were dried in vacuo at 300 °C overnight before usage. All MOFs crystals were ground (for better doping or mixing) before CVD doping or mixing with Pt nanoparticles. Freshly made Pt nanoparticles were dispersed in about 1 mL of ethanol. The colloidal solution was then added into a small vial containing 0.2 g of predried HKUST-1. The mixture was ultrasonicated for 15 min and dried in a 60 °C oven. Before further experiments, the obtained Pt-HKUST-1 was subject to evacuation at 160 °C to remove residual ethanol. Pt-MIL-53 and Pt-ZIF-8 were obtained by following the same procedure. The Pt contents in HKUST-1, MIL-53, and ZIF-8 were estimated to be about 5.2% in HKUST-1, 5.0% in MIL-53, and 5.3% in ZIF-8 by XPS analysis, respectively.

2.1.4. Hydrogenation Experiments of Pt-HKUST-1, Pt-MIL-53, and Pt-ZIF-8. Pt-HKUST-1 obtained by incipient wetness method was transferred onto a quartz boat and then placed in a horizontal furnace tube. The furnace tube was sealed and purged with H_2 at a flow rate of 60 cm^3/min. The sample was heated from room temperature at a constant heating rate of 2 °C/min to 150 °C and held at 150 °C for 16 h. After that, the sample was cooled down to room temperature, purged with N_2 for 1 h, and then subject to evacuation at 160 °C overnight before further measurements. The sample obtained by this way was denoted as Pt-HKU-150. For Pt-HKUST-1 samples subject to other H_2 treatment temperatures of 100, 75, 50, and 25 °C were denoted as Pt-HKU-100, Pt-HKU-75, Pt-HKU-50, and Pt-HKU-25, respectively. Following the same approach, HKUST-1 processed at 150 and 100 °C was denoted as HKU-150 and HKU-100. MIL-53, ZIF-8, Pt-MIL-53, and Pt-ZIF-8 were also processed by the same procedure but only treated in H_2 at 150 °C, which were denoted as MIL-53-150, ZIF-8-150, Pt-MIL-53-150, and Pt-ZIF-8-150, respectively. In our previous study, it was shown that the spillover equilibrium on MOFs was completed within 5 h at room temperature, thus 16 h was sufficient for reaching equilibrium of hydrogen spillover on these samples.[61]

All synthesized H_2-treated samples were stored in desiccators to minimize exposure to ambient air before being subjected to XPS and other measurements.

2.1.5. Synthesis of Pt-HKUST-1 via Chemical Vapor Deposition (CVD). Pt was doped on HKUST-1 by chemical vapor deposition of a volatile platinum precursor (trimethyl)-methylcyclopentadienylplatinum(IV). The detailed procedure was reported in our previous work.[98] HKUST-1 was ground before CVD. The grounded HKUST-1 (0.6 g) and the organometallic precursor (0.09 g) were placed in a tube separated by a glass frit and degassed to a vacuum of <10 μmHg at 0 °C. After that, the degassing was stopped and temperature was increased to 30 °C and held at 30 °C for 1 h. The evauation of this system was renewed every hour for six cycles and then stayed for another 6 h. The yielded composite was reduced in a hydrogen atmosphere at 150 °C overnight and then purged with flowing helium. The obtained Pt-HKUST-1 by this way was designated as Pt-HKU-CVD.

2.2. Sample Characterization and Isotherm Measurements. Powder X-ray diffraction (XRD) data were recorded on a Rigaku rotating anode X-ray diffractometer at 40 kV, 100 mA for Cu Kα (λ = 0.1541 nm) radiation, with a step size of 0.02° in 2θ. All the XRD patterns were obtained on the ground MOFs and doped MOFs because a flat surface of sample is needed for XRD analysis. X-ray photoelectron spectroscopy (XPS) and X-ray-excited Auger electron spectroscopy (XAES) data were recorded on a Kratos Axis ultra XPS spectrometer (mono Al source) at 14 kV, 8 mA, with a resolution of pass energy 10 eV. BET (Brunauer−Emmett−Teller) surface areas were measured with a standard static volumetric technique (Micromeritics ASAP2020).

3. RESULTS AND DISCUSSION

Conventional method for doping metal nanoparticles onto MOFs usually involves two steps: infiltration of metal precursors into frameworks followed by reduction of the metal precursor in an H_2 atmosphere at one specific high temperature (e.g., 200 °C).[75,77,78] Since the obtained metal-doped MOFs have been treated in H_2 at high temperature, one cannot examine the stabilities of MOFs in H_2 at the temperature lower than the reduction temperature. In order to study the stabilities of MOFs at various temperatures, a new method is used in this study; i.e., colloidal Pt nanoparticles were synthesized by ethylene glycol reduction, and then the reduced Pt nanoparticle was doped on MOFs via incipient wetness impregnation at room temperature. The operation at room temperature allowed us to study the stabilities of doped MOFs in H_2 at various temperatures.

Structural losses of porous materials including MOFs are commonly studied using powder XRD and surface area measurements. For example, Long's group used XRD and BET surface area to estimate the structural changes of MOF-5 by different preparation and handling methods,[11] and Walton el al. also used XRD and BET surface area to study the structural degradation of several MOFs exposed to water vapor.[90]

Powder X-ray diffraction patterns of as-obtained HKUST-1, HKU-100, and HKU-150 are shown in Figure 1. The pristine HKUST-1 consists of a face-centered cubic crystal lattice of

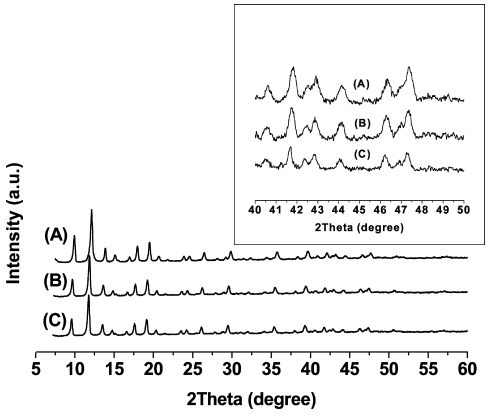

Figure 1. XRD patterns of (A) HKUST-1, (B) HKU-100, and (C) HKU-150; inset figure magnifies XRD patterns ranged from 40° to 50° in 2θ.

dx.doi.org/10.1021/jp401367k | J. Phys. Chem. C 2013, 117, 7565−7576

$Fm\bar{3}m$ space group and possesses typical peaks at 2θ = 9.5° (220), 11.7° (222), 13.5° (400), 14.7° (331), 16.5°(422), 17.5° (511), and 19.1° (440), which is in good agreement with previous reports.[92,93,99] After being exposed in hydrogen environment at 100 and 150 °C for 16 h, HKU-100 and HKU-150 exhibited the same peaks with those of pristine HKUST-1, although the peak intensity decreased slightly. BET surface area measurements also showed that the surface area of HKUST-1 dropped slightly from 1150 m^2/g to 992 and 901 m^2/g after being treated in hydrogen atmosphere at 100 and 150 °C for 16 h, respectively. This means the major crystalline integrity of HKUST-1 remained intact after exposure to hydrogen molecules at elevated temperatures.

Lueking et al. showed that hydrogenation of HKUST-1 mixed with Pt/C catalyst happened to carboxylate groups and not aromatic carbons, but the valence state of copper in HKUST-1 remained unknown.[92] In order to investigate the state of copper cluster, X-ray photoelectron spectroscopy was conducted around the characteristic peak range of copper, 930−965 eV. The X-ray photoelectron spectra of HKUST-1, HKU-100, and HKU-150 are shown in Figure 2. Two

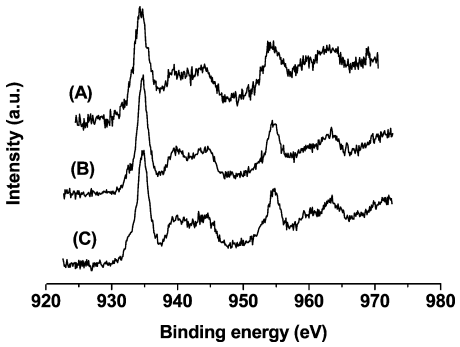

Figure 2. Cu 2p XPS spectra of pristine HKUST-1 and HKUST-1 processed in H_2 at 100 and 150 °C for 16 h: (A) HKUST-1, (B) HKU-100, and (C) HKU-150.

characteristic peaks of divalent Cu^{2+} were observed at 934.6 and 954.4 eV, corresponding to Cu $2p_{3/2}$ and Cu $2p_{1/2}$, respectively.[100−102] Meanwhile, the presence of the well-known "shake-up satellites" (which are the other peaks appeared in the range of 930−965 eV except the two characteristic peaks) found in Cu spectra is generally considered as an indication of the presence of Cu(II) species.[103−107] We note that there was also a very small, barely noticeable Cu^0 shoulder at 932 eV in Cu 2p XPS of HKU-100 and HKU-150. This was caused by partial Cu reduction (a very small fraction). However, all these results indicated almost all copper element in HKUST-1 remained as divalent state after exposure to hydrogen at elevated temperatures for a prolonged time, which means pristine HKUST-1 is stable in H_2 up to 150 °C.

Since dissociated hydrogen with unshared electrons possess higher chemical reactivity than stable dihydrogen molecules,[108] it is important to investigate the stability of HKUST-1 in the presence of dissociated hydrogen although the stabilities in dihydrogen environment at elevated temperatures have been verified above. In order to induce dissociated hydrogen to MOFs, Pt nanoparticles were doped onto HKUST-1 by the incipient wetness method as described in the Experimental Section. Hydrogen molecules first chemisorbed and dissociated on the surface of Pt and then migrated from Pt surface to the surface of HKUST-1 followed by surface diffusion. The resulting HKUST-1 samples treated with dissociated hydrogen were examined by XRD and XPS. Powder XRD patterns of pristine HKUST-1 and Pt-doped HKUST-1 before and after H_2 treatment at 150 °C are shown in Figure 3.

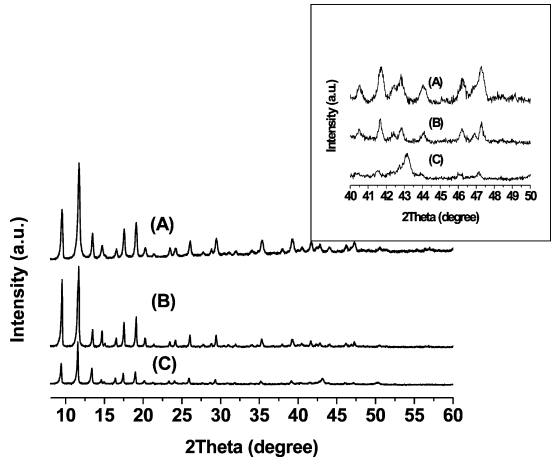

Figure 3. XRD patterns of (A) HKUST-1, (B) Pt-HKUST-1 before H_2 treatment, and (C) Pt-HKU-150; inset figure magnifies XRD patterns ranged from 40° to 50° in 2θ.

As shown in Figure 3, the peak intensity of Pt-HKUST-1 was slightly lower than that of pristine HKUST-1. Nitrogen adsorption results also showed that the surface area of HKUST-1 decreased from 1150 to 960 m^2/g after Pt-doping procedure. The lower surface area of Pt-HKUST-1 than HKUST-1 was due to the increased weight and the pore blocking of HKUST-1 caused by Pt nanoparticles. TEM image of Pt-HKUST-1 showed that Pt nanoparticles of slightly below 1 to ∼10 nm were doped on the crystal of HKUST-1 (Figure S1 in Supporting Information). It is worth noting that the decrease in BET surface area of MOFs after metal-doping procedure is a normal phenomenon reported in many previous studies.[74−76,78,109,110] The surface areas of MOFs before and after metal doping observed in previous literature and our work are compared in Table 1 below.

Table 1. Surface Area of MOFs before and after Metal Doping: (a) Langmuir Surface Area; (b) BET Surface Area

sample	doped metal	doped amount (wt %)	surface area of pristine MOF (m^2/g)	surface area of doped MOF (m^2/g)	ref
MOF-5	Pd	3	718	452[a]	109
SNU-3	Pd	3	559	242[b]	76
MIL-100	Pd	10	1200	380[b]	75
IRMOF-8	Pt	4.8	1430	1175[a]	78
MOF-5	Ru	30	3300	860[a]	110
MOF-177	Pt	43	5600	867[b]	74
HKUST-1	Pt	5	1150	960[b]	this work

Although the peak intensity and BET surface area of HKUST-1 decreased after Pt-doping, the structure of HKUST-1 was retained, and no extra peak appeared in XRD pattern. However, after being subjected to H_2 treatment at 150 °C for 16 h, the peak intensities of Pt-HKUST-1 declined substantially. This was also confirmed by BET surface area measurement: BET surface area of Pt-HKUST-1 dropped

dx.doi.org/10.1021/jp401367k | J. Phys. Chem. C 2013, 117, 7565−7576

severely from 960 to 151 m^2/g upon H_2 treatment at 150 °C. Moreover, a new strong peak around 2θ = 43.2° emerged (shown in inset figure), which is a characteristic peak of Cu^0 species at the (111) plane.[111−114] Compared with the inset figure in Figure 1, we could find that pristine HKUST-1 without Pt nanoparticles retained its microstructure and copper element in HKUST-1 remained as divalent state after being subjected to H_2 treatment at 150 °C, while a large part of Pt-HKUST-1 structure collapsed and part of divalent copper Cu^{2+} in HKUST-1 was reduced to metallic copper Cu^0. This indicates that HKUST-1 is not stable in the presence of dissociated hydrogen generated by hydrogen spillover, although HKUST-1 showed good resistance to the dihydrogen atmosphere. This is because dissociated hydrogen with an unshared electron are much more reactive and thus a much more effective reducing agent than dihydrogen molecules. Dissociated hydrogen can easily attack and break the coordinated bonding between Cu and O, which led to the reduction of divalent copper element.

To confirm that the severe structural loss of Pt-HKUST-1 was caused by the dissociated hydrogen rather than the heating in inert gas (i.e., that Pt-HKUST-1 is thermally stable at 150 °C), Pt-HKUST-1 was heated at 150 °C for 16 h in N_2 instead of H_2. As shown in Figures S3 and S4, no new peak appeared in the XRD pattern of Pt-HKUST-1 and the valence state of Cu in Pt-HKUST-1 remained unchanged after the treatment in N_2 at 150 °C. The surface area of Pt-HKUST-1 remained at 960 m^2/g.

To further investigate the temperature effects on hydrogen spillover and the stabilities of MOFs, Pt-doped HKUST-1 samples were treated at various temperatures and the XRD patterns of the treated samples in the range of 41°−50° in 2θ were displayed in Figure 4 (XRD patterns of samples in full range of 5°−60° in 2θ are shown in Figure S2).

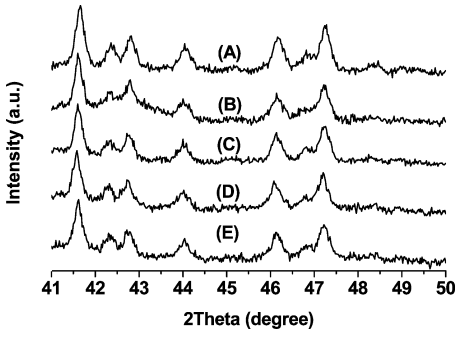

Figure 4. XRD patterns ranged from 41° to 50° in 2θ for (A) Pt-HKUST-1 before H_2 treatment, (B) Pt-HKU-100, (C) Pt-HKU-75, (D) Pt-HKU-50, and (E) Pt-HKU-25.

Compared with XRD pattern of Pt-HKU-150, the peak at 43.2° shrunk into a small hump in the XRD pattern of Pt-HKU-100. When H_2 treatment temperatures were lowered to 75, 50, and 25 °C, the peak at 43.2° became more unclear in the XRD patterns of Pt-HKU-75, Pt-HKU-50, and Pt-HKU-25. This is reasonable and could be explained by the decreased chemical activities of dissociated hydrogen with temperature decreased. In order to examine the states of Cu elements in these samples, X-ray photoelectron spectroscopy was conducted around the characteristic peak range of copper, 930−965 eV, and the corresponding X-ray photoelectron spectra are shown in Figure 5.

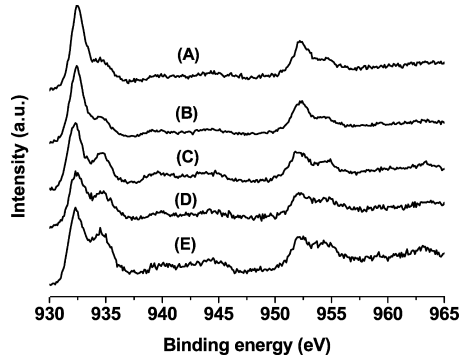

Figure 5. Cu 2p XPS spectra of Pt-HKUST-1 processed in H_2 at 150, 100, 75, 50, and 25 °C for 16 h: (A) Pt-HKU-150, (B) Pt-HKU-100, (C) Pt-HKU-75, (D) Pt-HKU-50, and (E) Pt-HKU-25.

As illustrated in Figure 2, pristine HKUST-1 processed in H_2 at 150 and 100 °C showed two major characteristic peaks of divalent Cu (Cu^{2+}) at 934.6 and 954.4 eV with a very small, barely noticeable Cu shoulder at 932 eV (Figure 2). This small, barely noticeable Cu shoulder was caused by partial Cu reduction (a very small fraction). However, when Pt-HKUST-1 treated in H_2 at different temperatures for 16 h, two intense, obvious peaks appeared at 932.4 and 952.2 eV, which can be assigned to Cu (0/1+).[115,116] Moreover, the intensity of "shake-up satellites" decreased much as an evidence of the reduction of divalent copper. One reasonable explanation is that hydrogen molecules chemisorbed and dissociated on the surface of Pt and then spilt over to surface of HKUST-1 and followed by surface diffusion on HKUST-1. The spiltover atomic hydrogen moved to the location of Cu−O coordination bonding and interacted with Cu−O, which led to the formation of lower-valence copper. Meanwhile, the ratio of Cu^{2+} peak area vs $Cu^{0/+}$ peak area decreased with the treatment temperature being increased, which demonstrates more divalent copper was reduced at higher temperatures, in consistent with the XRD results. Since it is difficult to distinguish between metallic Cu^0 and Cu^+ due to overlap of XPS spectra,[115,116] X-ray-excited Auger electron spectroscopy (XAES) of Cu LMM was carried out to distinguish Cu^0 and Cu^+, and the Cu LMM XAES spectrum of Pt-HKU-100 as an example is shown in Figure 6. In Figure 6, the peak around kinetic energy 918.6 eV was assigned to be Cu^0, while the peak around 917.5 eV was attributed to Cu^{2+}.[103] As for the peak at 915.0 eV, it is also related with Cu^0, although it is not always useful for chemical state determination.[115]

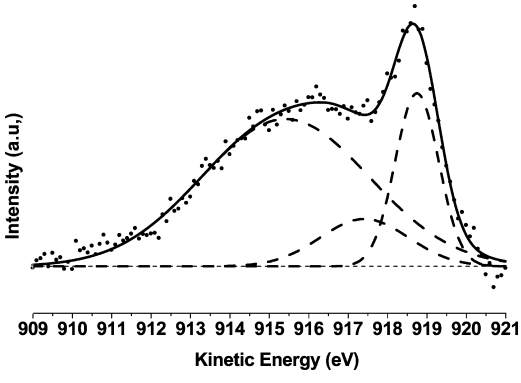

Figure 6. Cu LMM XAES spectrum of Pt-HKU-100.

dx.doi.org/10.1021/jp401367k | J. Phys. Chem. C 2013, 117, 7565−7576

For clarity, we also compared of XRD, BET surface area, and XPS of HKUST-1, Pt-HKUST-1, treated HKUST-1, and treated Pt-HKUST-1 (after being subjected to H_2 treatment at 150 °C for 16 h) in Table 2, which one can clearly see the huge differences among these untreated and treated MOFs.

Table 2. Comparison of XRD, BET Surface area, and XPS of HKUST-1, Pt-HKUST-1, Treated HKUST-1, and Treated Pt-HKUST-1 (After Being Subjected to H_2 Treatment at 150 °C for 16 h)

sample	XRD intensity	presence of Cu^0 at 2θ = 43.2° in XRD	BET surface area (m^2/g)	Cu^0 at 932 eV in Cu 2p XPS
HKUST-1	high	no	1150	no
Pt-HKUST-1	high	no	960	no
treated HKUST-1	slightly reduced	no	901	small, barely noticeable shoulder
treated Pt-HKUST-1	substantially reduced	yes	151	intense and major peak

This evidence also demonstrated that HKUST-1 tends to be hydrogenated by dissociated hydrogen more than by relatively stable dihydrogen molecules, since divalent copper in HKUST-1 remained intact in H_2 at 150 and 100 °C for 16 h while part of Cu^{2+} in Pt-HKUST-1 was reduced to Cu^0 in the presence of dissociated hydrogen at 100 °C.

Stabilities of MIL-53 were also examined by the same approaches. XRD patterns of MIL-53 samples before and after H_2 treatment at 150 °C (MIL-53 and MIL-53-150) and Pt-doped MIL-53 samples before and after H_2 treatment (Pt-MIL-53 and Pt-MIL-53−150) are shown in Figure 7.

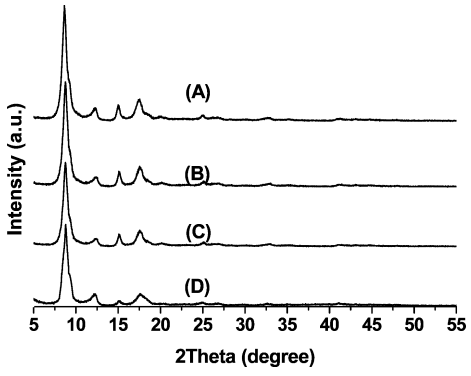

Figure 7. XRD patterns of (A) MIL-53, (B) MIL-53-150, (C) Pt-MIL-53, and (D) Pt-MIL-53-150.

The XRD pattern of pristine MIL-53 in Figure 7 is in good agreement with previous reports.[117,118] After being treated in H_2 at 150 °C for 16 h, no change was observed in XRD pattern of MIL-53-150, which demonstrated MIL-53 has good resistance toward H_2 under such a condition. After Pt-doping process, the peak intensity of MIL-53 decreased slightly, probably due to the pore blocking of MIL-53 by Pt nanoparticles. However, unlike Pt-HKUST-1, Pt-MIL-53 showed good stability and maintained crystalline integrity with dissociated hydrogen after being exposed in H_2 environment at 150 °C for 16 h, which was verified from the unaltered XRD pattern of Pt-MIL-53-150. Further tests of the states of aluminum elements in MIL-53, MIL-53-150, and Pt-MIL-53-150 conducted by XPS around Al 2s peak are shown in Figure 8.

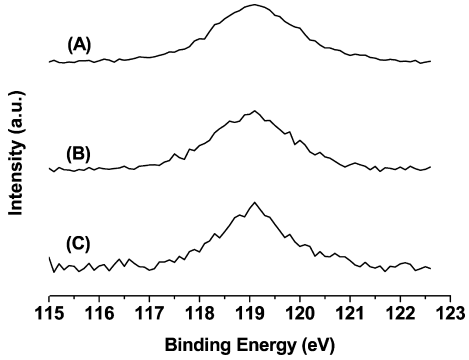

Figure 8. Al 2s XPS spectra of (A) MIL-53, (B) MIL-53-150, and (C) Pt-MIL-53-150.

In Figure 8, typical Al 2s peaks at 191.2 eV were observed for pristine MIL-53, which is the characteristic peak of Al^{3+}.[119,120] Although small changes of fwhm (full width at half-maximum) appeared, no peak shift for Al 2s was observed on MIL-53-150 and Pt-MIL-53-150, which demonstrates the state of aluminum elements in MIL-53 remain intact and reconfirmed our conclusion from XRD patterns that MIL-53 exhibited good stability in both dihydrogen and dissociated hydrogen environments at elevated temperatures. This is reasonable because Al possesses a much lower reduction potential than hydrogen.

Stabilities of ZIF-8 samples were also studied in dihydrogen and dissociated hydrogen environments. XRD patterns of ZIF-8 samples before and after H_2 treatment at 150 °C (ZIF-8 and ZIF-8-150) and Pt-doped ZIF-8 samples before and after H_2 treatment (Pt- ZIF-8 and Pt- ZIF-8-150) are shown in Figure 9.

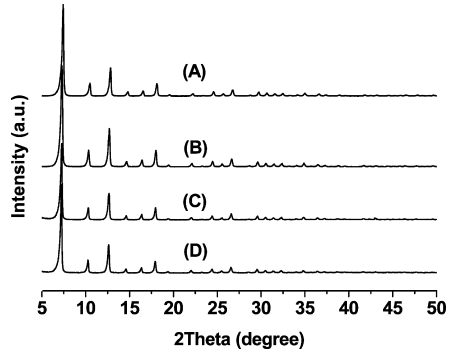

Figure 9. XRD patterns of ZIF-8 samples: (A) ZIF-8, (B) ZIF-8-150, (C) Pt-ZIF-8, and (D) Pt-ZIF-8-150.

In Figure 9, pristine ZIF-8 consists of a body-centered cubic (BCC) crystal lattice with reflections of (011), (002), (112), (022), (013), (222), (233), and (134) planes at 2θ = 7.4°, 10.4°, 12.8°, 14.7°, 16.5°, 18.1°, 24.6°, and 26.7°, respectively.[83,121] After being exposed in H_2 at 150 °C for 16 h, there was no peak change observed for ZIF-8-150, which demonstrated ZIF-8 also has a good stability in dihydrogen environment. XRD results also illustrated further doping Pt nanoparticles on ZIF-8 did not cause any structure alternation. Moreover, Pt-doped ZIF-8 still remained crystalline integrity after being treated in H_2 at 150 °C for 16 h, which manifests ZIF-8 is stable in both dihydrogen and dissociated hydrogen at

dx.doi.org/10.1021/jp401367k | J. Phys. Chem. C 2013, 117, 7565−7576

elevated temperatures. XPS measurements were also performed to verify the states of Zn elements in ZIF-8, ZIF-8-150, and Pt-ZIF-8-150, which are shown in Figure 10.

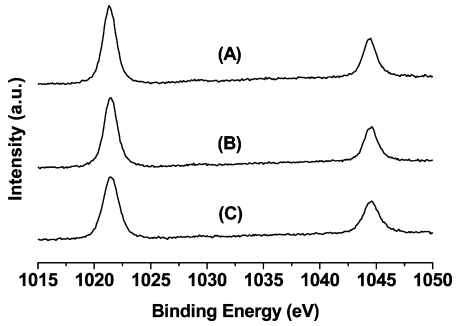

Figure 10. Zn 2p XPS spectra of (A) ZIF-8, (B) ZIF-8-150, and (C) Pt-ZIF-8-150.

As shown in Figure 10, two characteristic peaks of Zn were observed in the XPS spectra of pristine ZIF-8, where are at 1021.4 and 1044.5 eV corresponding to Zn $2p_{3/2}$ and Zn $2p_{1/2}$, respectively.[122−124] Since it is difficult to distinguish the oxidation states of Zn by only using Zn 2p spectra due to the overlap of binding energy range of Zn^0 and Zn^{2+},[124] Zn LMM Auger spectra were carried out to determine the chemical states of Zn, and the results are shown in Figure 11.

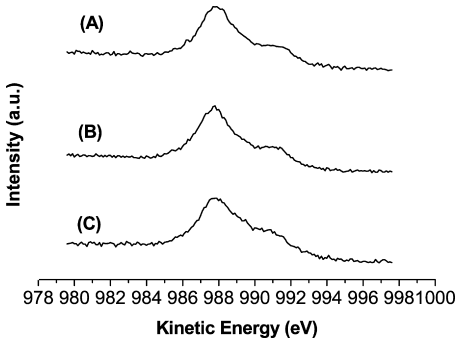

Figure 11. Zn LMM spectra of (A) ZIF-8, (B) ZIF-8-150, and (C) Pt-ZIF-8-150.

After being treated in H_2 at 150 °C for 16 h, no peak shifts were observed on both ZIF-8-150 and Pt-ZIF-8-150 in Figures 10 and 11, which confirms the valence states of Zn elements in ZIF-8 samples remained intact in the presence of H_2 and dissociated hydrogen. This is in good agreement with XRD results. This phenomenon could also be explained by the lower reduction potential of Zn than hydrogen, which means hydrogen cannot reduce the divalent Zn.

It is noted that Zn in ZIF-8 has no open coordination sites. The open metal sites are known to interact more strongly with adsorbate molecules than saturated metal sites. To see if the open sites affect the stability, Zn-MOF-74 with the open Zn sites was treated under the same conditions of ZIF-8. As shown in Figures S5 and S6, the open Zn sites in Zn-MOF-74 could not be reduced by hydrogen.

On the basis of the XRD and XPS results, it could be concluded that the stabilities of MOFs in the presence of H_2 or dissociated hydrogen are related to the reduction potentials of metal elements in MOFs. For metal elements like Zn or Al possessing much lower reduction potentials (−0.76 and −1.66 V, respectively) compared with hydrogen,[125,126] they could retain original valence states after contact with H_2 or dissociated hydrogen even at elevated temperatures. But for the MOFs with metal elements like Cu, which has a slightly higher reduction potential (+0.34 V) compared with hydrogen,[127] they can basically remain intact in dihydrogen molecules environment, but they would lose structure when exposed to the more reactive dissociated hydrogen. The degree of hydrogenation is also related with temperature. More structural loss was observed at higher temperatures in the presence of dissociated hydrogen, as shown in the XRD patterns of Pt-HKUST-1 processed at different temperatures.

One important factor affecting the hydrogen spillover is the contact between dissociation metals and receptors.[128,129] More intimate contacts between the metal and carbon led to a lower energy barrier for the spillover of dissociated hydrogen from Pt to carbon.[129] As shown above, Pt-HKUST-1 would lose part of crystalline integrity after contact with hydrogen atoms at elevated temperatures. Thus, the effect of contact on hydrogen spillover could be evaluated by the degree of collapse in the crystal structure of Pt-HKUST-1 via two different synthesis methods: incipient wetness doping and organometallic chemical vapor deposition.

Powder X-ray diffraction patterns of pristine HKUST-1 and Pt-HKU-CVD are shown in Figure 12. As shown in Figure 12,

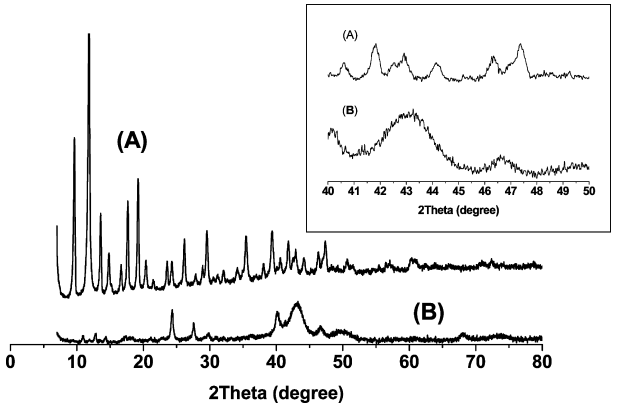

Figure 12. XRD patterns of (A) HKUST-1 and (B) Pt-HKU-CVD; inset figure shows XRD patterns of these two samples from 40° to 50° in 2θ.

the crystal structure of pristine HKUST-1 severely collapsed after doping and reducing Pt-precursor by the CVD method. Most characteristic peaks of pristine HKUST-1 disappeared during the CVD doping process. Moreover, a pronounced peak at 2θ = 43.2° emerged, which is the characteristic peak of Cu^0 species at (111) plane.[111−114] This demonstrates that the majority part of divalent Cu in HKUST-1 was reduced to metallic Cu^0 by spilt-over dissociated hydrogen generated on the surface of Pt in the CVD reduction process. The severe collapse was confirmed by BET measurements, which showed the surface area of treated Pt-HKU-CVD dropped dramatically from 1150 to 15 m^2/g.

In Figure 3, part of Pt-HKUST-1 structure exhibited peak variance, since the positions of most peaks remained intact in XRD patterns while the XRD intensity and BET surface area decreased less substantially compared with Pt-HKU-CVD. This is a distinct proof that contact between metals and receptors plays an important role in hydrogen spillover. To synthesize Pt-HKU-CVD, Pt was first doped on HKUST-1 by vapor

dx.doi.org/10.1021/jp401367k | J. Phys. Chem. C 2013, 117, 7565−7576

deposition of a volatile platinum precursor (trimethyl)-methylcyclopentadienylplatinum(IV), and then the Pt organo-precursor decomposed and was reduced by H_2 into metallic Pt on the surface of HKUST-1. Because of the in-situ reduction and growth of metallic Pt on the surface of HKUST-1 framework, the contact between Pt nanoparticles and HKUST-1 receptor is much more intimate than the doping of colloidal Pt nanoparticles on HKUST-1 via incipient wetness. Thus, it facilitated the migration of dissociated hydrogen from Pt surface to HKUST-1 framework surface and subsequently caused more severe hydrogenation of HKUST-1 framework due to more Cu−O bonding breaking in the presence of more migrated dissociated hydrogen. Meanwhile, the XRD pattern of Pt-HKU-CVD also supports our conclusion that HKUST-1 is not stable in contact with dissociated hydrogen at elevated temperatures. It is worth noting that our previous results showed the crystal structures of Pt-doped IRMOF-8 (Zn cluster) prepared via the same CVD method remained intact.[78] The stability difference between Pt-HKU-CVD and Pt-IRMOF-8-CVD also confirms that the metal cluster in MOFs is a key factor influencing the stability of MOFs in the presence of dissociated hydrogen due to different reduction potentials of different metal elements.

We also measured the hydrogen uptakes on HKUST-1, untreated/fresh Pt-HKUST-1 (never seen hydrogen before the measurement), and treated Pt-HKUST-1 (treated in H_2 at 150 °C for 16 h). As shown in Figure S7, hydrogen uptake on fresh Pt-HKUST-1 was 1.5 times that on HKUST-1. The 50% enhancement on fresh Pt-HKUST-1 was contributed by hydrogen adsorption on Pt and spilt-over hydrogen adsorption on HKUST-1. Note that hydrogen uptake on treated Pt-HKUST-1 was much less than that on fresh Pt-HKUST-1. This is because Pt-HKUST-1 degraded after being treated in H_2 at 150 °C for 16 h, and the surface area was reduced from 960 m^2/g (untreated Pt-HKUST-1) to 151 m^2/g (treated Pt-HKUST-1). It is interesting to note that hydrogen uptake on treated Pt-HKUST-1 was almost the same as that on HKUST-1, although the huge differences in their surface area, 151 m^2/g for treated Pt-HKUST-1 and 1150 m^2/g for HKUST-1. Obviously, the spillover enhancement on treated Pt-HKUST-1 offset the loss of hydrogen uptake by its low surface area. These results also indicated the hydrogen spillover occurred on Pt-HKUST-1.

Note that, as shown in Table 2, the huge differences between treated HKUST-1 and treated Pt-HKUST-1 were caused by the much higher activity of dissociated H than H_2 molecules. We conclude that reduction potential determines whether a metal can be reduced by hydrogen, and the forms of hydrogen, dissociated H atom, or hydrogen molecules affected how much/fast the Cu in HKUST-1 was reduced. That is why a very small, barely noticeable Cu^0 shoulder at 932 eV was observed in Cu 2p XPS of HKU-100 and HKU-150 (meaning a very small fraction of Cu was reduced), and two intense, major peaks at 932.4 and 952.2 eV, assigned to Cu (0/1+), were observed on Pt-HKUST-1 (meaning Cu in Pt-HKUST-1 was most/fast reduced). We emphasize that it is not "Pt speeding up kinetics of degradation" but the H atom dissociated by Pt caused the strong degradation of Pt-HKUST-1. If the degradation of Pt-HKUST-1 was caused by Pt not H, the other three MOFs doped with Pt should have shown degradation, but they did not. Also, the XPS results have confirmed the severe reduction of Cu (intense, obvious Cu^0 peak at 932 eV) in Pt-HKUST-1 (Cu can be reduced by H not by Pt), which consequently led to the reduced surface area of Pt-HKUST-1.

4. CONCLUSIONS

In this work, a series of Pt-doped HKUST-1, MIL-53, and ZIF-8 samples were synthesized via colloidal nanoparticles incipient wetness impregnation and the CVD method. Their stabilities in the presence of dihyrogen molecules and dissociated hydrogen were examined by XRD and XPS measurements. Al-based and Zn-based frameworks exhibited good stabilities in both dihydrogen molecules and dissociated hydrogen environments at elevated temperatures (up to 150 °C). The structure of Cu-based framework HKUST-1 remained intact in dihydrogen environment, but the structure of the Pt-doped HKUST-1 began to collapse upon exposure to H_2, as a result of spillover of the dissociated hydrogen. The degree of collapse increased with temperature. The stabilities of MOFs with different metal clusters in H_2 and dissociated hydrogen environments are related to the different reduction potentials of the metal elements. A further comparison of the stabilities of MOF-74 (with open coordination sites) and ZIF-8 (without open coordination sites) confirmed that the stability of MOF was related to reduction potential of metal in MOF not the presence/absence of open sites. This work provides useful information for future optimization of MOFs as hydrogen storage candidate materials, which should have good stabilities in the presence of H_2 or dissociated hydrogen at ambient as well as elevated temperatures. Moreover, significant difference in stabilities between Pt-HKU-CVD and Pt-HKU (via incipient wetness) showed that the contacts between Pt metal and the framework played an important role in hydrogen spillover.

■ ASSOCIATED CONTENT

Ⓢ Supporting Information

Experimental details; Figures S1−S7. This material is available free of charge via the Internet at http://pubs.acs.org.

■ AUTHOR INFORMATION

Corresponding Author

*E-mail yang@umich.edu; Tel (734) 936-0771; Fax (734) 764-7453.

Notes

The authors declare no competing financial interest.

■ ACKNOWLEDGMENTS

This work was supported by Ford University Research Program from Ford Motor Company and NSF grant CBET-0753008.

■ REFERENCES

(1) Schlapbach, L.; Zuttel, A. Hydrogen-Storage Materials for Mobile Applications. *Nature* **2001**, *414*, 353−358.

(2) Office of Power Delivery, Office of Power Technologies, Energy Efficiency and Renewable Energy, Department of Energy, Washington, D.C. *A Multiyear Plan for the Hydrogen R&D Program*, 1999.

(3) Dillon, A. C.; Jones, K. M.; Bekkedahl, T. A.; Kiang, C. H.; Bethune, D. S.; Heben, M. J. Storage of Hydrogen in Single-Walled Carbon Nanotubes. *Nature* **1997**, *386*, 377−379.

(4) Choi, M.; Ryoo, R. Mesoporous Carbons with KOH Activated Framework and their Hydrogen Adsorption. *J. Mater. Chem.* **2007**, *17*, 4204.

(5) Chen, H.; Yang, R. T. Catalytic Effects of TiF_3 on Hydrogen Spillover on Pt/Carbon for Hydrogen Storage. *Langmuir* **2010**, *26*, 15394−15398.

(6) Nishihara, H.; Hou, P. X.; Li, L. X.; Ito, M.; Uchiyama, M.; Kaburagi, T.; Ikura, A.; Katamura, J.; Kawarada, T.; Mizuuchi, K.; Kyotani, T. High-Pressure Hydrogen Storage in Zeolite-Templated Carbon. *J. Phys. Chem. C* **2009**, *113*, 3189−3196.
(7) Langmi, H. W.; Book, D.; Walton, A.; Johnson, S. R.; Al-Mamouri, M. M.; Speight, J. D.; Edwards, P. P.; Harris, I. R.; Anderson, P. A. Hydrogen Storage in Ion-Exchanged Zeolites. *J. Alloys Compd.* **2005**, *404*−*406*, 637−642.
(8) Zecchina, A.; Bordiga, S.; Vitillo, J. G.; Ricchiardi, G.; Lamberti, C.; Spoto, G.; Bjørgen, M.; Lillerud, K. P. Liquid Hydrogen in Protonic Chabazite. *J. Am. Chem. Soc.* **2005**, *127*, 6361−6366.
(9) Saha, D.; Deng, S. Hydrogen Adsorption on Ordered Mesoporous Carbons Doped with Pd, Pt, Ni, and Ru. *Langmuir* **2009**, *25*, 12550−12560.
(10) Parambhath, V. B.; Nagar, R.; Ramaprabhu, S. Effect of Nitrogen Doping on Hydrogen Storage Capacity of Palladium Decorated Graphene. *Langmuir* **2012**, *28*, 7826−7833.
(11) Kaye, S. S.; Dailly, A.; Yaghi, O. M.; Long, J. R. Impact of Preparation and Handling on the Hydrogen Storage Properties of Zn_4O(1,4-benzenedicarboxylate)$_3$ (MOF-5). *J. Am. Chem. Soc.* **2007**, *129*, 14176−14177.
(12) Murray, L. J.; Dinca, M.; Long, J. R. Hydrogen Storage in Metal-Organic Frameworks. *Chem. Soc. Rev.* **2009**, *38*, 1294.
(13) Dincă, M.; Dailly, A.; Liu, Y.; Brown, C. M.; Neumann, D. A.; Long, J. R. Hydrogen Storage in a Microporous Metal−Organic Framework with Exposed Mn^{2+} Coordination Sites. *J. Am. Chem. Soc.* **2006**, *128*, 16876−16883.
(14) Ma, S.; Zhou, H. C. A Metal−Organic Framework with Entatic Metal Centers Exhibiting High Gas Adsorption Affinity. *J. Am. Chem. Soc.* **2006**, *128*, 11734−11735.
(15) Ma, S. Q.; Sun, D. F.; Ambrogio, M.; Fillinger, J. A.; Parkin, S.; Zhou, H. C. Framework-catenation Isomerism in Metal-Organic Frameworks and Its Impact on Hydrogen Uptake. *J. Am. Chem. Soc.* **2007**, *129*, 1858−1859.
(16) Collins, D. J.; Zhou, H. C. Hydrogen Storage in Metal-Organic Frameworks. *J. Mater. Chem.* **2007**, *30*, 3154−3160.
(17) Chae, H.; Siberio-Perez, D. Y.; Kim, J.; Go, Y.; Eddaoudi, M.; Matzger, A.; O'Keeffe, M.; Yaghi, O. M. A Route to High Surface Area, Porosity and Inclusion of Large Molecules in Crystals. *Nature* **2004**, *427*, 523−527.
(18) Rowsell, J. L. C.; Yaghi, O. M. Effects of Functionalization, Catenation, and Variation of the Metal Oxide and Organic Linking Units on the Low-pressure Hydrogen Adsorption Properties of Metal-Organic Frameworks. *J. Am. Chem. Soc.* **2006**, *128*, 1304−1315.
(19) Frost, H.; Snurr, R. Q. Design Requirements for Metal-Organic Frameworks as Hydrogen Storage Materials. *J. Phys. Chem. C* **2007**, *111*, 18794−18803.
(20) Keskin, S.; Liu, J.; Rankin, R. B.; Johnson, J. K.; Sholl, D. S. Progress, Opportunities, and Challenges for Applying Atomically Detailed Modeling to Molecular Adsorption and Transport in Metal−Organic Framework Materials. *Ind. Eng. Chem. Res.* **2008**, *48*, 2355−2371.
(21) Watanabe, T.; Sholl, D. S. Molecular Chemisorption on Open Metal Sites in Cu-3(benzenetricarboxylate)(2): A Spatially Periodic Density Functional Theory Study. *J. Chem. Phys.* **2010**, 133.
(22) Walton, K. S.; Snurr, R. Q. Applicability of the BET Method for Determining Surface Areas of Microporous Metal-Organic Frameworks. *J. Am. Chem. Soc.* **2007**, *129*, 8552−8556.
(23) Cai, Y.; Zhang, Y.; Huang, Y.; Marder, S. R.; Walton, K. S. Impact of Alkyl-Functionalized BTC on Properties of Copper-Based Metal−Organic Frameworks. *Cryst. Growth Des.* **2012**, *12*, 3709−3713.
(24) Mu, B.; Schoenecker, P. M.; Walton, K. S. Gas Adsorption Study on Mesoporous Metal−Organic Framework UMCM-1. *J. Phys. Chem. C* **2010**, *114*, 6464−6471.
(25) Park, H. J.; Suh, M. P. Enhanced Isosteric Heat of H-2 Adsorption by Inclusion of Crown Ethers in a Porous Metal-organic Framework. *Chem. Commun.* **2012**, *48*, 3400−3402.
(26) Prasad, T. K.; Suh, M. P. Control of Interpenetration and Gas-Sorption Properties of Metal-Organic Frameworks by a Simple Change in Ligand Design. *Chem.—Eur. J.* **2012**, *18*, 8673−8680.
(27) Park, H. J.; Suh, M. P. Stepwise and Hysteretic Sorption of N-2, O-2, CO2, and H-2 Gases in a Porous Metal-Organic Framework Zn-2(BPnDC)(2)(bpy). *Chem. Commun* **2010**, *46*, 610−612.
(28) Prasad, T. K.; Hong, D. H.; Suh, M. P. High Gas Sorption and Metal-Ion Exchange of Microporous Metal-Organic Frameworks with Incorporated Imide Groups. *Chem.—Eur. J.* **2010**, *16*, 14043−14050.
(29) Latroche, M.; Surblé, S.; Serre, C.; Mellot-Draznieks, C.; Llewellyn, P. L.; Lee, J. H.; Chang, J. S.; Jhung, S. H.; Férey, G. Hydrogen Storage in the Giant-Pore Metal-Organic Frameworks MIL-100 and MIL-101. *Angew. Chem., Int. Ed.* **2006**, *45*, 8227−8231.
(30) Furukawa, H.; Miller, M.; Yaghi, O. M. Independent Verification of the Saturation Hydrogen Uptake in MOF-177 and Establishment of a Benchmark for Hydrogen Adsorption in Metal−Organic Frameworks. *J. Mater. Chem.* **2007**, *17*, 3197−3204.
(31) Koh, K.; Wong-Foy, A. G.; Matzger, A. J. A Porous Coordination Copolymer with over 5000 m^2/g BET Surface Area. *J. Am. Chem. Soc.* **2009**, *131*, 4184−4185.
(32) Furukawa, H.; Ko, N.; Go, Y. B.; Aratani, N.; Choi, S. B.; Choi, E.; Yazaydin, A. Ö.; Snurr, R. Q.; O'Keeffe, M.; Kim, J.; Yaghi, O. M. Ultrahigh Porosity in Metal-Organic Frameworks. *Science* **2010**, *329*, 424−428.
(33) Farha, O. K.; Özgür Yazaydın, A.; Eryazici, I.; Malliakas, C. D.; Hauser, B. G.; Kanatzidis, M. G.; Nguyen, S. T.; Snurr, R. Q.; Hupp, J. T. De Novo Synthesis of a Metal−Organic Framework Material Featuring Ultrahigh Surface Area and Gas Storage Capacities. *Nat. Chem.* **2010**, *2*, 944−948.
(34) Farha, O. K.; Eryazici, I.; Jeong, N. C.; Hauser, B. G.; Wilmer, C. E.; Sarjeant, A. A.; Snurr, R. Q.; Nguyen, S. T.; Yazaydin, A. O.; Hupp, J. T. Metal-Organic Framework Materials with Ultrahigh Surface Areas: Is the Sky the Limit? *J. Am. Chem. Soc.* **2012**, *134*, 15016−15021.
(35) Robell, A. J.; Ballou, E. V.; Boudart, M. Surface Diffusion of Hydrogen on Carbon. *J. Phys. Chem.* **1964**, *68*, 2748−2753.
(36) Srinivas, S. T.; Rao, P. K. Direct Observation of Hydrogen Spillover on Carbon-supported Platinum and Its Influence on the Hydrogenation of Benzene. *J. Catal.* **1994**, *148*, 470−477.
(37) Conner, W. C.; Falconer, J. L. Spillover in Heterogeneous Catalysis. *Chem. Rev.* **1995**, *95*, 759−788.
(38) Pajonk, G. M. Contribution of Spillover Effects to Heterogeneous Catalysis. *Appl. Catal., A* **2000**, *202*, 157−169.
(39) Wang, L.; Yang, R. T. Hydrogen Storage on Carbon-Based Adsorbents and Storage at Ambient Temperature by Hydrogen Spillover. *Catal. Rev.* **2010**, *52*, 411−461.
(40) Sinfelt, J. H.; Lucchesi, P. J. Kinetic Evidence for the Migration of Reactive Intermediates in Surface Catalysis. *J. Am. Chem. Soc.* **1963**, *85*, 3365−3367.
(41) Khoobiar, S. Particle to Particle Migration of Hydrogen Atoms on Platinum—Alumina Catalysts from Particle to Neighboring Particles. *J. Phys. Chem.* **1964**, *68*, 411−412.
(42) Pajonk, G. M.; Teichner, S. Catalytic Activity of Platinum on Delta-alumina in the Hydrogenation of Ethylene. I. Catalytic Activity of Non-calcined Catalyst. *J. Bull. Soc. Chim.* **1971**, 3847−3855.
(43) Benson, J. E.; Kohn, H. W.; Boudart, M. On the Reduction of Tungsten Trioxide Accelerated by Platinum and Water. *J. Catal.* **1966**, *5*, 307−313.
(44) Boudart, M.; Vannice, M. A.; Benson, J. E. Adlineation, Portholes and Spillover. *Z. Phys. Chem.* **1969**, *64*, 171−177.
(45) Sermon, P. A.; Bond, G. C. Hydrogen Spillover. *Catal. Rev.* **1974**, *8*, 211−239.
(46) Mitchell, P. C. H.; Ramirez-Cuesta, A. J.; Parker, S. F.; Tomkinson, J.; Thompsett, D. Hydrogen Spillover on Carbon-Supported Metal Catalysts Studied by Inelastic Neutron Scattering. Surface Vibrational States and Hydrogen Riding Modes. *J. Phys. Chem. B* **2003**, *107*, 6838−6845.
(47) Mitchell, P. C. H.; Ramirez-Cuesta, A. J.; Parker, S. F.; Tomkinson, J. Inelastic Neutron Scattering in Spectroscopic Studies of

Hydrogen on Carbon-Supported Catalytsts-Experimental Spectra and Computed Spectra of Model Systems. *J. Mol. Struct.* **2003**, *651*−*653*, 781−785.
(48) Tsao, C.-S.; Liu, Y.; Li, M.; Zhang, Y.; Leao, J. B.; Chang, H.-W.; Yu, M.-S.; Chen, S.-H. Neutron Scattering Methodology for Absolute Measurement of Room-Temperature Hydrogen Storage Capacity and Evidence for Spillover Effect in a Pt-Doped Activated Carbon. *J. Phys. Chem. Lett.* **2010**, *1*, 1569−1573.
(49) Tsao, C.-S.; Liu, Y.; Chuang, H.-Y.; Tseng, H.-H.; Chen, T.-Y.; Chen, C.-H.; Yu, M.-S.; Li, Q.; Lueking, A.; Chen, S.-H. Hydrogen Spillover Effect of Pt-Doped Activated Carbon Studied by Inelastic Neutron Scattering. *J. Phys. Chem. Lett.* **2011**, *2*, 2322−2325.
(50) Bhowmick, R.; Rajasekaran, S.; Friebel, D.; Beasley, C.; Jiao, L.; Ogasawara, H.; Dai, H.; Clemens, B.; Nilsson, A. Hydrogen Spillover in Pt-Single-Walled Carbon Nanotube Composites: Formation of Stable C−H Bonds. *J. Am. Chem. Soc.* **2011**, *133*, 5580−5586.
(51) Zhan, D. P.; Velmurugan, J.; Mirkin, M. V. Adsorption/Desorption of Hydrogen on Pt Nanoelectrodes: Evidence of Surface Diffusion and Spillover. *J. Am. Chem. Soc.* **2009**, *131*, 14756−14760.
(52) Panayotov, D. A.; Yates, J. T. Spectroscopic Detection of Hydrogen Atom Spillover from Au Nanoparticles Supported on TiO2: Use of Conduction Band Electrons. *J. Phys. Chem. C* **2007**, *111*, 2959−2964.
(53) Panayotov, D. A.; Burrows, S. P.; Yates, J. T.; Morris, J. R. Mechanistic Studies of Hydrogen Dissociation and Spillover on Au/TiO_2: IR Spectroscopy of Coadsorbed CO and H-Donated Electrons. *J. Phys. Chem. C* **2011**, *115*, 22400−22408.
(54) Chen, L.; Cooper, A. C.; Pez, G. P.; Cheng, H. Mechanistic Study on Hydrogen Spillover Onto Graphitic Carbon Materials. *J. Phys. Chem. C* **2007**, *111*, 18995−19000.
(55) Sha, X. W.; Knippenberg, M. T.; Cooper, A. C.; Pez, G. P.; Cheng, H. S. Dynamics of Hydrogen Spillover on Carbon-Based Materials. *J. Phys. Chem. C* **2008**, *112*, 17465−17470.
(56) Singh, A. K.; Ribas, M. A.; Yakobson, B. I. H-Spillover through the Catalyst Saturation: An Ab Initio Thermodynamics Study. *ACS Nano* **2009**, *3*, 1657−1662.
(57) Lin, Y.; Ding, F.; Yakobson, B. I. Hydrogen Storage by Spillover on Graphene as a Phase Nucleation Process. *Phys. Rev. B: Condens. Matter* **2008**, *78*, 04140201−04140204.
(58) Lee, K.; Kim, Y.-H.; Sun, Y. Y.; West, D.; Zhao, Y.; Chen, Z.; Zhang, S. B. Hole-Mediated Hydrogen Spillover Mechanism in Metal-Organic Frameworks. *Phys. Rev. Lett.* **2010**, *104*, 236101.
(59) Tsao, C. S.; Yu, M. S.; Wang, C. Y.; Liao, P. Y.; Chen, H. L.; Jeng, U. S.; Tzeng, Y. R.; Chung, T. Y.; Wut, H. C. Nanostructure and Hydrogen Spillover of Bridged Metal-Organic Frameworks. *J. Am. Chem. Soc.* **2009**, *131*, 1404−1405.
(60) Miller, M. A.; Wang, C. Y.; Merrill, G. N. Experimental and Theoretical Investigation Into Hydrogen Storage via Spillover in IRMOF-8. *J. Phys. Chem. C* **2009**, *113*, 3222−3231.
(61) Li, Y.; Yang, F. H.; Yang, R. T. Kinetics and Mechanistic Model for Hydrogen Spillover on Bridged Metal−Organic Frameworks. *J. Phys. Chem. C* **2007**, *111*, 3405−3411.
(62) Cao, W.; Li, Y.; Wang, L.; Liao, S. Effects of Metal Ions and Ligand Functionalization on Hydrogen Storage in Metal−Organic Frameworks by Spillover. *J. Phys. Chem. C* **2011**, *115*, 13829−13836.
(63) Suri, M.; Dornfeld, M.; Ganz, E. Calculation of Hydrogen Storage Capacity of Metal-Organic and Covalent-Organic Frameworks by Spillover. *J. Chem. Phys.* **2009**, *131*, 174703−174706.
(64) Ganz, E.; Dornfeld, M. Storage Capacity of Metal−Organic and Covalent−Organic Frameworks by Hydrogen Spillover. *J. Phys. Chem. C* **2012**, *116*, 3661−3666.
(65) Psofogiannakis, G. M.; Froudakis, G. E. Theoretical Explanation of Hydrogen Spillover in Metal−Organic Frameworks. *J. Phys. Chem. C* **2011**, *115*, 4047−4053.
(66) Li, Y.; Yang, R. T. Hydrogen Storage in Metal−Organic Frameworks by Bridged Hydrogen Spillover. *J. Am. Chem. Soc.* **2006**, *128*, 8136−8137.
(67) Wang, C.-Y.; Tsao, C.-S.; Yu, M.-S.; Liao, P.-Y.; Chung, T.-Y.; Wu, H.-C.; Miller, M. A.; Tzeng, Y.-R. Hydrogen Storage Measurement, Synthesis and Characterization of Metal−Organic Frameworks via Bridged Spillover. *J. Alloys Compd.* **2010**, *492*, 88−94.
(68) Stuckert, N. R.; Wang, L.; Yang, R. T. Characteristics of Hydrogen Storage by Spillover on Pt-Doped Carbon and Catalyst-Bridged Metal Organic Framework. *Langmuir* **2010**, *26*, 11963−11971.
(69) Anbia, M.; Mandegarzad, S. Enhanced Hydrogen Sorption on Modified MIL-101 with Pt/CMK-3 by Hydrogen Spillover Effect. *J. Alloys Compd.* **2012**, *532* (0), 61−67.
(70) Lin, K.-S.; Adhikari, A. K.; Chang, K.-C.; Tu, M.-T.; Lu, W. Hydrogen Adsorption in Metal Organic Frameworks by Hydrogen Spillover. *Catal. Today* **2011**, *164* (1), 23−27.
(71) Yang, S. J.; Choi, J. Y.; Chae, H. K.; Cho, J. H.; Nahm, K. S.; Park, C. R. Preparation and Enhanced Hydrostability and Hydrogen Storage Capacity of CNT@MOF-5 Hybrid Composite. *Chem. Mater.* **2009**, *21*, 1893−1897.
(72) Lee, S.-Y.; Park, S.-J. Effect of Platinum Doping of Activated Carbon on Hydrogen Storage Behaviors of Metal-Organic Frameworks-5. *Int. J. Hydrogen Energy* **2011**, *36*, 8381−8387.
(73) Liu, Y. Y.; Zhang, J.; Zeng, J. L.; Chu, H. L.; Xu, F.; Sun, L. X. Hydrogen Storage Capacity of Nickel Supported on a Metal-Organic Framework Compound under Mild Conditions. *Chin. J. Catal.* **2008**, *29*, 655−659.
(74) Proch, S.; Herrmannsdorfer, J.; Kempe, R.; Kern, C.; Jess, A.; Seyfarth, L.; Senker, J. Pt@MOF-177: Synthesis, Room-temperature Hydrogen Storage and Oxidation Catalysis. *Chem.—Eur. J.* **2008**, *14*, 8204−12.
(75) Zlotea, C.; Campesi, R.; Cuevas, F.; Leroy, E.; Dibandjo, P.; Volkringer, C.; Loiseau, T.; Ferey, G.; Latroche, M. Pd Nanoparticles Embedded into a Metal-Organic Framework: Synthesis, Structural Characteristics, and Hydrogen Sorption Properties. *J. Am. Chem. Soc.* **2010**, *132*, 2991−2997.
(76) Cheon, Y. E.; Suh, M. P. Enhanced Hydrogen Storage by Palladium Nanoparticles Fabricated in a Redox-Active Metal-Organic Framework. *Angew. Chem., Int. Ed.* **2009**, *48*, 2899−903.
(77) Sabo, M.; Henschel, A.; Frode, H.; Klemm, E.; Kaskel, S. Solution Infiltration of Palladium into MOF-5: Synthesis, Physisorption and Catalytic Properties. *J. Mater. Chem.* **2007**, *17*, 3827−3832.
(78) Wang, L. F.; Stuckert, N. R.; Chen, H.; Yang, R. T. Effects of Pt Particle Size on Hydrogen Storage on Pt-Doped Metal-Organic Framework IRMOF-8. *J. Phys. Chem. C* **2011**, *115*, 4793−4799.
(79) Moon, H. R.; Kim, J. H.; Suh, M. P. Redox-Active Porous Metal-Organic Framework Producing Silver Nanoparticles from Ag-I Ions at Room Temperature. *Angew. Chem., Int. Ed.* **2005**, *44*, 1261−1265.
(80) Suh, M. P.; Moon, H. R.; Lee, E. Y.; Jang, S. Y. A Redox-Active Two-Dimensional Coordination Polymer: Preparation of Silver and Gold Nanoparticles and Crystal Dynamics on Guest Removal. *J. Am. Chem. Soc.* **2006**, *128*, 4710−4718.
(81) Kalidindi, S. B.; Oh, H.; Hirscher, M.; Esken, D.; Wiktor, C.; Turner, S.; Van Tendeloo, G.; Fischer, R. A. Metal@COFs: Covalent Organic Frameworks as Templates for Pd Nanoparticles and Hydrogen Storage Properties of Pd@COF-102 Hybrid Material. *Chem. (Weinheim an der Bergstrasse, Germany)* **2012**, *18*, 10848−56.
(82) Suh, M. P.; Park, H. J.; Prasad, T. K.; Lim, D.-W. Hydrogen Storage in Metal−Organic Frameworks. *Chem. Rev.* **2011**, *112*, 782−835.
(83) Park, K. S.; Ni, Z.; Côté, A. P.; Choi, J. Y.; Huang, R.; Uribe-Romo, F. J.; Chae, H. K.; O'Keeffe, M.; Yaghi, O. M. Exceptional Chemical and Thermal Stability of Zeolitic Imidazolate Frameworks. *Proc. Natl. Acad. Sci. U. S. A.* **2006**, *103*, 10186−10191.
(84) Choi, H. J.; Dinca, M.; Dailly, A.; Long, J. R. Hydrogen Storage in Water-Stable Metal-Organic Frameworks Incorporating 1,3- and 1,4-Benzenedipyrazolate. *Energy Environ. Sci* **2010**, *3*, 117−123.
(85) Wu, T.; Shen, L.; Luebbers, M.; Hu, C.; Chen, Q.; Ni, Z.; Masel, R. I. Enhancing the Stability of Metal-Organic Frameworks in Humid Air by Incorporating Water Repellent Functional Groups. *Chem. Commun.* **2010**, *46*, 6120−6122.
(86) Han, S. S.; Choi, S.-H.; van Duin, A. C. T. Molecular Dynamics Simulations of Stability of Metal-Organic Frameworks against H2O

Using the ReaxFF Reactive Force Field. *Chem. Commun.* **2010**, *46*, 5713−5715.
(87) Saha, D.; Deng, S. Structural Stability of Metal Organic Framework MOF-177. *J. Phys. Chem. Lett.* **2009**, *1*, 73−78.
(88) Saha, D.; Deng, S. Ammonia Adsorption and Its Effects on Framework Stability of MOF-5 and MOF-177. *J. Colloid Interface Sci.* **2010**, *348*, 615−620.
(89) Kang, I. J.; Khan, N. A.; Haque, E.; Jhung, S. H. Chemical and Thermal Stability of Isotypic Metal−Organic Frameworks: Effect of Metal Ions. *Chem.—Eur. J.* **2011**, *17*, 6437−6442.
(90) Schoenecker, P. M.; Carson, C. G.; Jasuja, H.; Flemming, C. J. J.; Walton, K. S. Effect of Water Adsorption on Retention of Structure and Surface Area of Metal-Organic Frameworks. *Ind. Eng. Chem. Res.* **2012**, *51*, 6513−6519.
(91) Mu, B.; Walton, K. S. Thermal Analysis and Heat Capacity Study of Metal−Organic Frameworks. *J. Phys. Chem. C* **2011**, *115*, 22748−22754.
(92) Liu, X. M.; Rather, S.-u.; Li, Q.; Lueking, A.; Zhao, Y.; Li, J. Hydrogenation of CuBTC Framework with the Introduction of a PtC Hydrogen Spillover Catalyst. *J. Phys. Chem. C* **2011**, *116*, 3477−3485.
(93) Li, Y.; Yang, R. T. Hydrogen Storage in Metal-Organic and Covalent-Organic Frameworks by Spillover. *AIChE J.* **2008**, *54*, 269−279.
(94) Chui, S. S. A Chemically Functionalizable Nanoporous Material $[Cu_3(TMA)_2(H_2O)_3]_n$. *Science* **1999**, *283*, 1148−1150.
(95) Rioux, R. M.; Song, H.; Hoefelmeyer, J. D.; Yang, P.; Somorjai, G. A. High-Surface-Area Catalyst Design: Synthesis, Characterization, and Reaction Studies of Platinum Nanoparticles in Mesoporous SBA-15 Silica. *J. Phys. Chem. B* **2005**, *109*, 2192−2202.
(96) Navin, J. K.; Grass, M. E.; Somorjai, G. A.; Marsh, A. L. Characterization of Colloidal Platinum Nanoparticles by MALDI-TOF Mass Spectrometry. *Anal. Chem.* **2009**, *81* (15), 6295−6299.
(97) Wang, Y.; Ren, J. W.; Deng, K.; Gui, L. L.; Tang, Y. Q. Preparation of Tractable Platinum, Rhodium, and Ruthenium Nanoclusters with Small ParticleSize in Organic Media. *Chem. Mater.* **2000**, *12*, 1622−1627.
(98) Wang, L.; Stuckert, N. R.; Chen, H.; Yang, R. T. Effects of Pt Particle Size on Hydrogen Storage on Pt-Doped Metal−Organic Framework IRMOF-8. *J. Phys. Chem. C* **2011**, *115*, 4793−4799.
(99) Carbonell, C.; Imaz, I.; Maspoch, D. Single-Crystal Metal−Organic Framework Arrays. *J. Am. Chem. Soc.* **2011**, *133*, 2144−2147.
(100) Peng, L.; Zhang, J.; Li, J.; Han, B.; Xue, Z.; Yang, G. Surfactant-Directed Assembly of Mesoporous Metal-Organic Framework Nanoplates in Ionic Liquids. *Chem. Commun.* **2012**, *48*, 8688−8690.
(101) Hanke, M.; Arslan, H. K.; Bauer, S.; Zybaylo, O.; Christophis, C.; Gliemann, H.; Rosenhahn, A.; Wöll, C. The Biocompatibility of Metal−Organic Framework Coatings: An Investigation on the Stability of SURMOFs with Regard to Water and Selected Cell Culture Media. *Langmuir* **2012**, *28*, 6877−6884.
(102) Biesinger, M. C.; Lau, L. W. M.; Gerson, A. R.; Smart, R. S. C. Resolving Surface Chemical States in XPS Analysis of First Row Transition Metals, Oxides and Hydroxides: Sc, Ti, V, Cu and Zn. *Appl. Surf. Sci.* **2010**, *257*, 887−898.
(103) Poulston, S.; Parlett, P. M.; Stone, P.; Bowker, M. Surface Oxidation and Reduction of CuO and Cu_2O Studied Using XPS and XAES. *Surf. Interface Anal.* **1996**, *24*, 811−820.
(104) Velásquez, P.; Leinen, D.; Pascual, J.; Ramos-Barrado, J. R.; Grez, P.; Gómez, H.; Schrebler, R.; Del Río, R.; Córdova, R. A Chemical, Morphological, and Electrochemical (XPS, SEM/EDX, CV, and EIS) Analysis of Electrochemically Modified Electrode Surfaces of Natural Chalcopyrite ($CuFeS_2$) and Pyrite (FeS_2) in Alkaline Solutions. *J. Phys. Chem. B* **2005**, *109*, 4977−4988.
(105) Kundakovic, L.; Flytzani-Stephanopoulos, M. Reduction Characteristics of Copper Oxide in Cerium and Zirconium Oxide Systems. *Appl. Catal., A* **1998**, *171*, 13−29.
(106) Otamiri, J. C.; Andersson, S. L. T.; Andersson, A. Ammoxidation of Toluene by $YBa_2Cu_3O_{6+x}$ and Copper oxides: Activity and XPS Studies. *Appl. Catal.* **1990**, *65*, 159−174.
(107) Meda, L.; Cerofolini, G. F. A Decomposition Procedure for the Determination of Copper Oxidation States in Cu-zeolites by XPS. *Surf. Interface Anal.* **2004**, *36*, 756−759.
(108) Laborda, F.; Bolea, E.; Baranguan, M. T.; Castillo, J. R. Hydride Generation in Anal. Chem. and Nascent Hydrogen: When Is It Going to Be Over? *Spectrochim. Acta, Part B* **2002**, *57*, 797−802.
(109) Dang, T. T.; Zhu, Y.; Ghosh, S. C.; Chen, A.; Chai, C. L. L.; Seayad, A. M. Atmospheric Pressure Aminocarbonylation of Aryl Iodides Using Palladium Nanoparticles Supported on MOF-5. *Chem. Commun.* **2012**, *48*, 1805−1807.
(110) Schröder, F.; Esken, D.; Cokoja, M.; van den Berg, M. W. E.; Lebedev, O. I.; Van Tendeloo, G.; Walaszek, B.; Buntkowsky, G.; Limbach, H.-H.; Chaudret, B.; Fischer, R. A. Ruthenium Nanoparticles inside Porous $[Zn_4O(bdc)_3]$ by Hydrogenolysis of Adsorbed [Ru(cod)(cot)]: A Solid-State Reference System for Surfactant-Stabilized Ruthenium Colloids. *J. Am. Chem. Soc.* **2008**, *130*, 6119−6130.
(111) Zhang, J. Y.; Liu, Y.; Chen, J.; Chen, Y.; Liu, G.; Zhang, X.; Sun, J. Mechanical Properties of Crystalline Cu/Zr and Crystal−Amorphous Cu/Cu−Zr Multilayers. *Mater. Sci. Eng., A* **2012**, *552*, 392−398.
(112) Reddy, K. M.; Gledhill, A. D.; Chen, C.-H.; Drexler, J. M.; Padture, N. P. High Quality, Transferrable Graphene Grown on Single Crystal Cu(111) Thin Films on Basal-Plane Sapphire. *Appl. Phys. Lett.* **2011**, *98*, 113117−3.
(113) Hayes, J. R.; Nyce, G. W.; Kuntz, J. D.; Satcher, J. H.; Hamza, A. V. Synthesis of Bi-Modal Nanoporous Cu, CuO and Cu_2O Monoliths with Tailored Porosity. *Nanotechnology* **2007**, *18*, 275602.
(114) Hansen, B. J.; Lu, G.; Chen, J. Direct Oxidation Growth of CuO Nanowires from Copper-Containing Substrates. *J. Nanomaterials* **2008**, *2008*, 1−7.
(115) Zhang, G.; Long, J.; Wang, X.; Dai, W.; Li, Z.; Wu, L.; Fu, X. Controlled Synthesis of Pure and Highly Dispersive Cu(ii), Cu(i), and Cu(0)/MCM-41 with $Cu[OCHMeCH_2NMe_2]_2$/MCM-41 as Precursor. *New J. Chem.* **2009**, *33*, 2044−2050.
(116) Chusuei, C. C.; Brookshier, M. A.; Goodman, D. W. Correlation of Relative X-ray Photoelectron Spectroscopy Shake-up Intensity with CuO Particle Size. *Langmuir* **1999**, *15*, 2806−2808.
(117) Loiseau, T.; Serre, C.; Huguenard, C.; Fink, G.; Taulelle, F.; Henry, M.; Bataille, T.; Férey, G. A Rationale for the Large Breathing of the Porous Aluminum Terephthalate (MIL-53) Upon Hydration. *Chem.—Eur. J.* **2004**, *10*, 1373−1382.
(118) Kubo, M.; Shimojima, A.; Okubo, T. Effect of Lithium Doping into MIL-53(Al) through Thermal Decomposition of Anion Species on Hydrogen Adsorption. *J. Phys. Chem. C* **2012**, *116*, 10260−10265.
(119) Rastomjee, C. S.; Keil, M.; Sotobayashi, H.; Bradshaw, A. M.; Lamont, C. L. A.; Gador, D.; Umbach, E. Aluminium Metallisation of Argon and Oxygen Plasma-Modified Polycarbonate Thin Film Surfaces. *Appl. Surf. Sci.* **1998**, *136*, 280−297.
(120) Sygellou, L.; Gianneta, V.; Xanthopoulos, N.; Skarlatos, D.; Georga, S.; Krontiras, C.; Ladas, S.; Kennou, S. ZrO_2 and Al_2O_3 Thin Films on Ge(100) Grown by ALD: An XPS Investigation. *Surf. Sci. Spectra* **2011**, *18*, 58−67.
(121) Xie, Z.; Yang, J.; Wang, J.; Bai, J.; Yin, H.; Yuan, B.; Lu, J.; Zhang, Y.; Zhou, L.; Duan, C. Deposition of Chemically Modified [small alpha]-Al_2O_3 Particles for High Performance ZIF-8 Membrane on a Macroporous Tube. *Chem. Commun.* **2012**, *48*, 5977−5979.
(122) Lupan, O.; Emelchenko, G. A.; Ursaki, V. V.; Chai, G.; Redkin, A. N.; Gruzintsev, A. N.; Tiginyanu, I. M.; Chow, L.; Ono, L. K.; Roldan Cuenya, B.; Heinrich, H.; Yakimov, E. E. Synthesis and Characterization of ZnO Nanowires for Nanosensor Applications. *Mater. Res. Bull.* **2010**, *45*, 1026−1032.
(123) Ali, Z.; Cha, S. N.; Sohn, J. I.; Shakir, I.; Yan, C.; Kim, J. M.; Kang, D. J. Design and Evaluation of Novel Zn Doped Mesoporous TiO_2 Based Anode Material for Advanced Lithium Ion Batteries. *J. Mater. Chem.* **2012**, *22*, 17625−17629.
(124) Min, Y. S.; An, C. J.; Kim, S. K.; Song, J.; Hwang, C. S. Growth and Characterization of Conducting ZnO Thin Films by Atomic Layer Deposition. *Bull. Korean Chem. Soc.* **2010**, *31*, 2503−2508.

(125) Haynes, W. M.; Lide, D. R.; Bruno, T. J. *CRC Handbook of Chemistry and Physics*; CRC Press: Boca Raton, FL, 2012.
(126) Lide, D. R. *CRC Handbook of Chemistry and Physics: A Ready-reference Book of Chemical and Physical Data*; CRC Press: Boca Raton, FL, 2006.
(127) Bard, A. J.; Parsons, R.; Jordan, J. *Standard Potentials in Aqueous Solution*; M. Dekker: New York, 1985.
(128) Wang, L. F.; Yang, R. T. Hydrogen Storage Properties of Carbons Doped with Ruthenium, Platinum, and Nickel Nanoparticles. *J. Phys. Chem. C* **2008**, *112*, 12486−12494.
(129) Wang, Z.; Yang, R. T. Enhanced Hydrogen Storage on Pt-Doped Carbon by Plasma Reduction. *J. Phys. Chem. C* **2010**, *114*, 5956−5963.